1972-01

Quasi-Geostrophic versus N on-Geostrophic Frontogenesis

Williams, R.T.

Journal of the Atmospheric Sciences, Volume 29, No. 1, January 1972, pp. 3-10.
http://hdl.handle.net/10945/45777

Quasi-Geostrophic versus Non-Geostrophic Frontogenesis

R. T. WILLIAMS

Dept. of Meteorology, Naval Postgraduate School, Monterey, Calif.

(Manuscript received 10 May 1971, in revised form 19 August 1971)

ABSTRACT

This study examines frontogenesis which is forced by a nondivergent horizontal wind field which contains stretching deformation. The initial conditions are formulated in such a way that the departures from the basic wind field are independent of x. The linear and nonlinear hydrostatic primitive equations are solved numerically and the solutions are compared. The linear solutions are very close to the solutions of the quasi-geostrophic equations. The latter equations predict fronts which have some unrealistic features and these equations predict discontinuities only for very large time. The nonlinear solutions are much more realistic than the linear solutions and they imply the formation of discontinuities within a finite period of time.

1. Introduction

Recent studies have shown that nondivergent horizontal wind deformation fields can produce zones of large temperature gradient. This process arises from either shearing or stretching deformation wind fields. Both effects occur in a typical baroclinic wave and Stone (1969) has shown that they are about equally important in frontogenesis. It is useful to analyze the shearing and stretching effects separately with idealized models. Arakawa (1962) and Williams (1967) examined the shearing mechanism with models which included vertical deformation fields. Stone (1966) and Williams and Plotkin (1968) studied the stretching mechanism with the quasi-geostrophic equations; these equations do not properly represent the vertical deformation effects. In this paper the earlier studies of the stretching mechanism will be generalized to include effects neglected in the quasi-geostrophic equations.

The quasi-geostrophic frontogenesis examined by Stone (1966) and Williams and Plotkin (1968) is unrealistic in certain respects. The predicted frontal zone does not tilt with height and this leads to superadiabatic lapse rates on the warm air side of the surface front. The maximum tangential velocities occur in the center of the frontal zone and the maximum speed in this jet tends to infinity as time increases. The vorticity is zero in the center of the frontal zone because the jet is symmetric. A temperature discontinuity forms only at the surface and only asymoptically for large time. The non-geostrophic study of the shearing deformation mechanism by Williams (1967) did not contain any of these unrealistic features. Thus, we expect that the addition of the non-geostrophic effects will considerably improve the stretching deformation solutions.

We can include the complete vertical deformation effects in our equations if the divergent part of the wind is included in the advection terms in the equations. The importance of the divergent component of the horizontal advection is proportional to the Rossby number [$\mathrm{Ro}=V/(fL)$, where V is the velocity scale and L the space scale; see Charney (1962) and Phillips (1963)]. For large-scale flow Ro is normally small. The quasi-geostrophic equations are obtained by neglecting all terms which are of order Ro or smaller. During frontogenesis the local Rossby number will increase due to a decrease in the scale L and/or an increase in V. Thus, the terms neglected in the quasi-geostrophic equations will become important in the latter stages of frontogenesis. The balance equations (Charney, 1962) include these effects, but they are not convenient for numerical solution. In this study we will employ the hydrostatic primitive equations because they are easier to solve numerically and because they are more general.

In Section 2, the Boussinesq equations are given and the modeling relations are introduced. In the model the time-dependent quantities are functions of y and z only. The basic wind deformation field is independent of time and height. The finite-difference approximations and boundary conditions are discussed in Section 3. The initial conditions are given in Section 4 and the numerical solutions are presented and discussed in Section 5. Both the linearized and the full nonlinear equations are solved numerically. Since the linear solutions are nearly equivalent to the quasi-geostrophic solutions, the difference between the linear and nonlinear solutions is due to non-geostrophic effects. The nonlinear solutions are much more realistic with respect

to their spatial structure and their time dependence. In Section 6 conclusions and suggestions for further work are given.

2. Basic equations

In this study we employ the Boussinesq equations, and we place our domain between two rigid horizontal planes. The compressibility of the atmosphere, which is neglected in the Boussinesq approximation, should not be of qualitative importance since the density scale height in the atmosphere is much larger than the thickness of typical frontal zones. The replacement of the tropopause by a rigid horizontal surface can be expected to give large errors in that region, but the resulting errors near the lower boundary should be small. These approximations were used in the other papers on frontogenesis which were discussed in Section 1.

The hydrostatic Boussinesq equations can be written in the following form when the earth's rotation is included:

$$\frac{\partial}{\partial t}\mathbf{V}+\nabla\cdot(\mathbf{V}\mathbf{V})+\frac{\partial}{\partial z}(w\mathbf{V})+\nabla\phi+f\mathbf{k}\times\mathbf{V}=0, \tag{2.1}$$

$$\frac{\partial\theta}{\partial t}+\nabla\cdot(\theta\mathbf{V})+\frac{\partial(w\theta)}{\partial z}=0, \tag{2.2}$$

$$\nabla\cdot\mathbf{V}+\frac{\partial w}{\partial z}=0, \tag{2.3}$$

$$\frac{\partial\phi}{\partial z}=g\theta/\theta_0, \tag{2.4}$$

where θ_0 is a constant reference potential temperature, p_0 a constant reference pressure, $\kappa=R/(Cp)$, $\theta=T(p_0/p)^\kappa-\theta_0$, the departure of the potential temperature from θ_0, and $\phi=Cp\theta_0(p/p_0)^\kappa+gz$, the pressure function. Heating and friction have been neglected in these equations although they may be important under certain conditions.

An exact steady solution to this set of equations is given by

$$\left.\begin{aligned}&\mathbf{V}=D(x\mathbf{i}-y\mathbf{j})\\&w=0\\&\phi=\Phi\equiv[-D^2(x^2+y^2)/2]-fDxy\\&\theta=0\end{aligned}\right\}, \tag{2.5}$$

where D is a constant. Cartesian coordinates have been introduced and f is taken to be constant. The horizontal velocity is a field of pure deformation and this deformation is given by $2D$. This is the basic velocity field which was used by Williams and Plotkin (1968).

If departures from the fields (2.5) are independent of x, then they will remain independent of x. Thus, we subdivide our dependent variables as follows:

$$\left.\begin{aligned}&\mathbf{V}=[Dx+u(y,z,t)]\mathbf{i}+[-Dy+v(y,z,t)]\mathbf{j}\\&w=w(y,z,t)\\&\theta=\theta(y,z,t)\\&\phi=\Phi(x,y)+\pi(y,z,t)\end{aligned}\right\}. \tag{2.6}$$

If we substitute these expressions into Eqs. (2.1)–(2.4), they become:

$$\frac{\partial u}{\partial t}+\frac{\partial(vu)}{\partial y}+\frac{\partial(wu)}{\partial z}-\frac{\partial V}{\partial y}u+V\frac{\partial u}{\partial y}-fv=0, \tag{2.7}$$

$$\frac{\partial v}{\partial t}+\frac{\partial(vv)}{\partial y}+\frac{\partial(wv)}{\partial z}+\frac{\partial}{\partial y}(vV)+\frac{\partial\pi}{\partial y}+fu=0, \tag{2.8}$$

$$\frac{\partial\theta}{\partial t}+\frac{\partial(v\theta)}{\partial y}+\frac{\partial}{\partial z}(w\theta)+V\frac{\partial\theta}{\partial y}=0, \tag{2.9}$$

$$\frac{\partial v}{\partial y}+\frac{\partial w}{\partial z}=0, \tag{2.10}$$

$$\frac{\partial\pi}{\partial z}=\frac{g\theta}{\theta_0}, \tag{2.11}$$

where $V=-Dy$. The boundary conditions are

$$w=0,\quad z=0,H, \tag{2.12}$$

where H is the distance between the horizontal plates.

If we define the vertical average of a quantity as

$$\langle(\ )\rangle\equiv\frac{1}{H}\int_0^H(\ )dz,$$

and integrate the hydrostatic equation (2.11) with respect to z and remove the vertical mean, we obtain

$$\pi-\langle\pi\rangle=\frac{g}{\theta_0}\left[\int_0^z\theta dz-\left\langle\int_0^z\theta dz\right\rangle\right]. \tag{2.13}$$

We now rewrite the y equation of motion in terms of $\pi-\langle\pi\rangle$. If we take the vertical average of (2.10) and use the boundary conditions (2.12), we obtain

$$\frac{\partial}{\partial y}\langle v\rangle=0.$$

This equation states that the total disturbance y mass flux is independent of y. If the other variables have proper symmetry it follows that $\langle v\rangle$ must be an odd function of y which leads to

$$\langle v\rangle=0. \tag{2.14}$$

If we take the vertical average of (2.8) and use (2.12) and (2.14), we obtain

$$\frac{\partial\langle vv\rangle}{\partial y}+\frac{\partial\langle\pi\rangle}{\partial y}+f\langle u\rangle=0. \tag{2.15}$$

When this result is subtracted from (2.8), we have

$$\frac{\partial}{\partial t}v+\frac{\partial}{\partial y}(vv-\langle vv\rangle)+\frac{\partial}{\partial z}(wv)+\frac{\partial}{\partial y}(vV)+\frac{\partial}{\partial y}(\pi-\langle\pi\rangle)+f(u-\langle u\rangle)=0. \quad (2.16)$$

Eqs. (2.7), (2.9), (2.10), (2.13) and (2.16) form a complete set which can be solved by a pure marching process.

3. Numerical procedure and boundary conditions

The arrangement of variables and the finite-difference approximations are the same as those used by Williams (1967). In order to close the problem computational boundaries must be introduced in y. Since the disturbance velocities should die out at a sufficient distance from the axis of dilatation, we set

$$v(\pm Y, z, t)=0. \quad (3.1)$$

However, there is appreciable inflow across these computational boundaries since $V(\pm Y)=\pm DY$. The quantities u and θ which are advected across the boundaries must be specified independent of the interior values if computational stability is to be maintained (Platzman, 1954). Thus, the following boundary conditions are used:

$$\left.\begin{aligned} u[\pm(Y+\Delta y/2),z,t]&=u[\pm(Y+\Delta y/2),z,0]\\ \theta[\pm(Y+\Delta y/2),z,t]&=\theta[\pm(Y+\Delta y/2),z,0]\end{aligned}\right\}. \quad (3.2)$$

The computational boundaries $y=\pm Y$ are placed between grid points so that the above conditions are actually applied at $y=\pm(Y+\Delta y/2)$.

These boundary conditions were found to be satisfactory, except that a weak nonlinear instability developed near the boundaries. This was removed by introducing a forward step every 72 time steps (see Arakawa, 1966, and Lilly, 1965).

4. Initial conditions

The initial temperature field is given by

$$\theta(y,z,0)=(\partial\bar{\theta}_I/\partial z)(z-H/2)-A(2/\pi)\arctan(\sinh\alpha y), \quad (4.1)$$

where $\alpha=f\pi H^{-1}(g\theta_0^{-1}\partial\bar{\theta}_I/\partial z)^{-\frac{1}{2}}$. The quantity $\partial\bar{\theta}_I/\partial z$, which is constant, is the initial stability and A is one-half the total horizontal temperature variation. Williams (1968) has obtained the following quasi-geostrophic solution for this initial temperature field:

$$\theta(y,z,\infty)=(\partial\bar{\theta}_I/\partial z)(z-H/2)-A(2/\pi)\arctan\left[\frac{\sinh\alpha y}{\sin(\pi z/H)}\right]. \quad (4.2)$$

The horizontal temperature variation described in (4.1) is independent of z and equal to the temperature distribution in the quasi-geostrophic solution at $z=H/2$. This initial temperature field was chosen so that the initial temperature on the plane $z=H/2$ would be near the limiting distribution for large time. Near the boundaries large temperature changes are expected since even the quasi-geostrophic solution is discontinuous at $y=0$, $z=0$ and $y=0$, $z=H$.

The initial x component of the velocity is given by

$$u(y,z,0)=-\frac{2}{\pi}\frac{gA\alpha}{f\theta_0}(z-H/2)\operatorname{sech}(\alpha y). \quad (4.3)$$

This field is obtained by substituting (4.1) into the thermal wind equation and integrating. The condition $u(y,H/2,0)=0$ is imposed to make the initial wind field antisymmetric in z. The y scale of initial θ and u fields is the Rossby radius of deformation, and this makes the initial conditions very much like a realistic portion of a finite-amplitude baroclinic wave.

Phillips (1960) has shown that gravity waves are suppressed in primitive equation forecasts if the quasi-geostrophic divergence is included in the initial wind field. In our model u is the rotational part of the wind and v is the divergent part. We will determine the initial V field from the quasi-geostrophic equations. In this case the quasi-geostrophic equations can be written as (Williams, 1967):

$$\frac{\partial u}{\partial t}+V\frac{\partial u}{\partial y}-\frac{\partial V}{\partial y}u-fv=0, \quad (4.4)$$

$$\frac{\partial\pi}{\partial y}+fu=0, \quad (4.5)$$

$$\frac{\partial\theta}{\partial t}+V\frac{\partial\theta}{\partial y}+\frac{\partial\bar{\theta}_I}{\partial z}w=0, \quad (4.6)$$

$$\frac{\partial v}{\partial y}+\frac{\partial w}{\partial z}=0, \quad (4.7)$$

$$\frac{\partial\pi}{\partial z}=\frac{g\theta}{\theta_0}. \quad (4.8)$$

If we introduce a streamfunction in the y-z plane, then (4.7) will be satisfied if we write

$$v=-\partial\Psi/\partial z \quad \text{and} \quad w=\partial\Psi/\partial y. \quad (4.9)$$

When these expressions are inserted into the above equations, they can be combined to give

$$\frac{1}{f^2}\frac{g}{\theta_0}\frac{\partial\bar{\theta}_I}{\partial z}\frac{\partial^2\Psi}{\partial y^2}+\frac{\partial^2\Psi}{\partial z^2}=\frac{2D}{f^2\theta_0}\frac{\partial\theta}{\partial y}. \quad (4.10)$$

This equation is solved for ψ from the initial temperature field (4.1) with the technique of Ogura and Charney (1962).

5. Numerical solutions

The finite-difference forms of Eqs. (2.7), (2.9), (2.10), (2.13) and (2.16) are solved by a pure marching process. It is instructive to compare these complete solutions with the quasi-geostropic solutions. A good approximation to the quasi-geostrophic predictions can be obtained from the linearized complete equations. The linearized equations are obtained by neglecting the second and third terms in (2.7) and (2.16), and by replacing θ with $\bar{\theta}_I$ in the second and third terms in (2.9). The resulting set of equations is the same as the quasi-geostrophic equations (4.4)–(4.8), with the exception of two linear terms which appear in the y-momentum equation. These terms allow for gravity waves, but these waves are not observed in the numerical solutions except near the boundaries. The nonlinear and linear equations are solved with the same finite-difference approximations. The differences between these numerical solutions will be due to the terms which are neglected in the quasi-geostrophic approximation.

All numerical results to be shown use the following numerical values for the constants:

$$\left.\begin{aligned} &f=10^{-4}\ \text{sec}^{-1}, \quad g/\theta_0=0.0327\ \text{m sec}^{-2}(^\circ\text{K})^{-1} \\ &H=9\ \text{km}, \quad Y=1800\ \text{km} \\ &D=10^{-5}\ \text{sec}^{-1}, \quad \partial\bar{\theta}_I/\partial z=4\text{K km}^{-1} \\ &A=12.56\text{K} \end{aligned}\right\}. \tag{5.1}$$

The following finite-difference increments are used:

$$\Delta y=20\ \text{km}, \quad \Delta z=333\ \text{m}, \quad \Delta t=200\ \text{sec}.$$

Some experiments with different values of the increments will be discussed later.

Fig. 1a contains the initial fields as a function of y at $z=167$ m, the lowest prediction level. The potential temperature departure ($\theta'=\theta-\bar{\theta}_I$) is antisymmetric in y and the maximum temperature gradient occurs at $y=0$. The velocity components u and v are symmetric about $y=0$ and they have maximum magnitudes at that point. These velocities are plotted on different scales since u is the rotational part of the wind and v is the divergent part. Fig. 1b shows the same fields predicted by the linear equations for $t=30$ hr. The new fields have the same symmetry properties as the initial fields so that the maximum temperature gradient and the maximum wind speeds occur at $y=0$. These symmetry features have been noted previously with quasi-geostrophic solutions by Stone (1966) and Williams and Plotkin (1968). The figure shows that the temperature gradient and the wind speeds have all increased from the initial state. The small oscillations in v which are present near the two computational boundaries ($y=\pm 1800$ km) represent gravity waves which are excited by the inexactness of the boundary conditions. These oscillations are not present in the central region where the frontogenesis is occurring. The nonlinear solutions at $t=30$ hr are shown in Fig. 1c. All fields

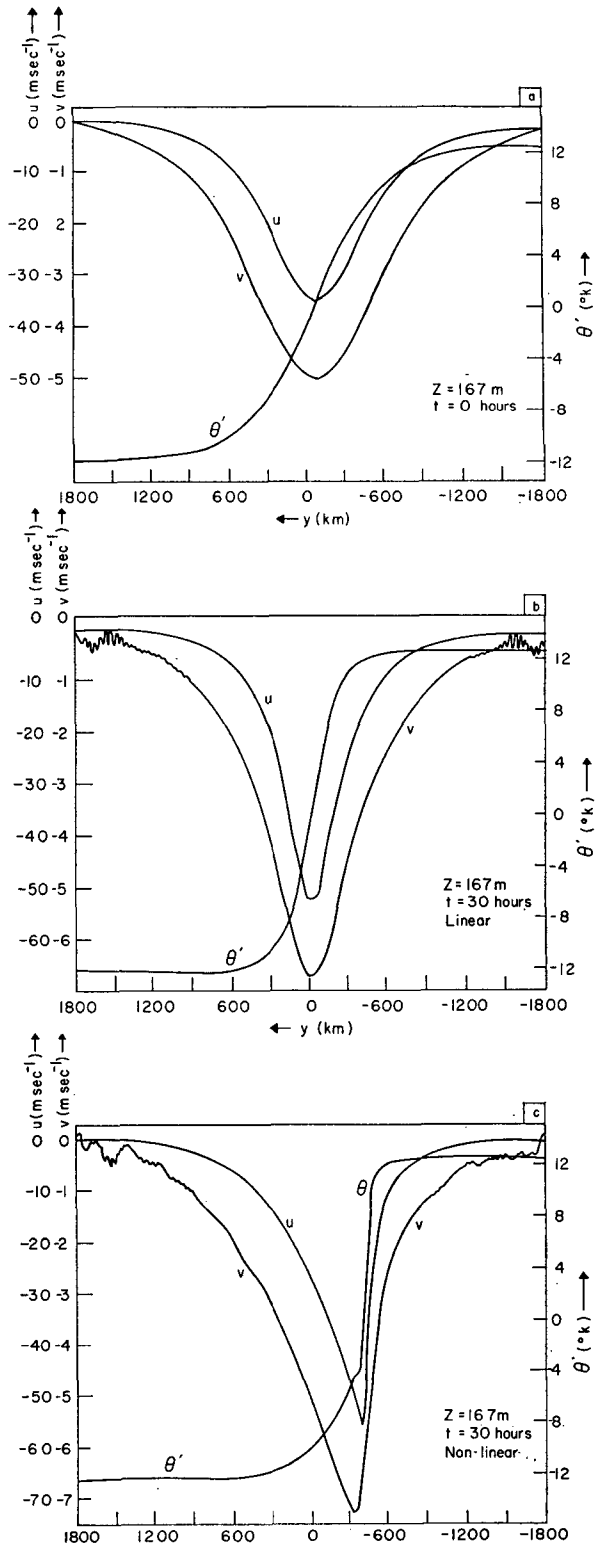

FIG. 1. The fields u, v and $\theta'=\theta-\bar{\theta}_I$ as functions of y at $z=167$ m. Fig. 1a contains the initial fields, 1b the fields predicted with the linear equations at $t=30$ hr and 1c the fields predicted with the nonlinear equations at $t=30$ hr.

contain asymmetries and the gradients are larger than the gradients predicted by the linear equations. The maximum temperature gradient is much larger than the value in Fig. 1b, and its location is shifted to $y\approx -400$ km from its initial location at $y=0$. It will be seen that this shift is indicative of a tilt of the frontal zone with height. The u field displays a very large positive vorticity in the region where the temperature gradient is the largest. This feature of atmospheric fronts is not predicted by the quasi-geostrophic equations; Fig. 1b shows a vorticity of zero in the center of the frontal zone surrounded by zones of large positive and negative vorticity. The v field shows large horizontal convergence in the frontal zone. These relationships between the temperature gradient, vorticity and divergence were noted in the non-geostrophic frontogenesis study by Williams (1967). In the previous study the frontogenesis arose from shearing deformation.

We now examine in more detail the differences between the frontogenesis rates of the linear and nonlinear equations. A reasonable measure of the width of the frontal zone is given by

$$d=\frac{\theta(-Y,z,0)-\theta(Y,z,0)}{|\partial\theta/\partial y|_{\max}}, \tag{5.2}$$

where $\partial\theta/\partial y$ is approximated by a one-sided difference. This type of expression was used by Williams (1967) as a measure of the frontal scale. Fig. 2 shows d as a function of time for both the linear and nonlinear solutions at $z=167$ m. The nonlinear solution has a smaller scale throughout the 3 days shown. In fact, at $t=30$ hr the nonlinear scale has been reduced by about one order of magnitude while the linear scale has been reduced by a factor of less than 3. Beyond 1.5 days the nonlinear solution contains considerable truncation error because the scale of the frontal zone is then of the order of the grid size. This error ultimately limits d to the order of the grid size. It was shown by Stone (1966) and by Williams and Plotkin (1968), with the quasi-geostrophic equations, that the maximum temperature gradient at $z=0$ increases as e^{DT}. This implies that d will asymptotically approach zero as $t\rightarrow\infty$. The curve for the linear solution in Fig. 2 shows this general type of behavior. If $z\neq 0$ it can be shown from Eq. (4.2) that d approaches the following value for large t:

$$d=d_0\sin(\pi z/H), \tag{5.3}$$

where $d_0=1022$ km. Thus, at $z=167$ m the limiting value is 59 km. At $t=4$ days (not shown) the linear solution gives $d=64$ km at this level which shows that the linear solution is gradually approaching the value given by (5.3).

Other numerical experiments were performed with the same initial conditions and with the following combinations of increments: $\Delta y=60$ km, $\Delta z=1000$ m, $\Delta t=600$ sec; $\Delta y=20$ km, $\Delta z=1000$ m, $\Delta t=200$ sec;

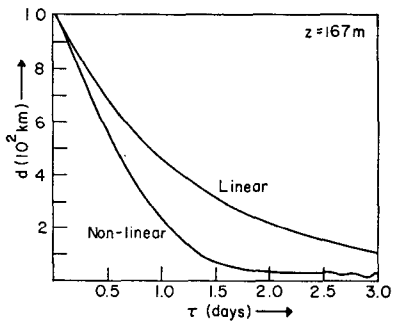

FIG. 2. Time variation of the frontal scale at $z=167$ m for the two experiments.

$\Delta y=60$ km, $\Delta z=333$ m, $\Delta t=600$ sec. The reduction in Δy produced only a small change in the d values for the linear solutions. A similarly small change was observed when Δz was decreased provided that the solutions were compared at the same z. These results indicate that the linear solutions shown are quite accurate. The nonlinear solutions displayed a decrease in d as Δy was reduced provided that Δz was sufficiently small. A reduction in d was also observed when Δz was decreased with z held fixed. These results suggest that the nonlinear solution is approaching a discontinuity. Some experiments were also performed to determine the influence of the boundary conditions at $y=\pm Y$. The nonlinear solutions were recomputed with $Y=1200$ km rather than 1800 km, and the difference within the frontal region were found to be quite small.

In order to isolate the nonlinear effects, Fig. 3 shows the ratio of the d values from the nonlinear solution to the d values from the linear solution. After a short adjustment period this ratio decreases linearly in t until $t\approx 1.5$ days. Beyond $t=1.5$ days the truncation error in the nonlinear solution limits further reduction in the ratio. Williams (1967) found that the nonlinear terms caused a similar decrease in scale in his study of a growing baroclinic wave (see Fig. 5 in that paper). His approximate analysis predicted a linear decrease in

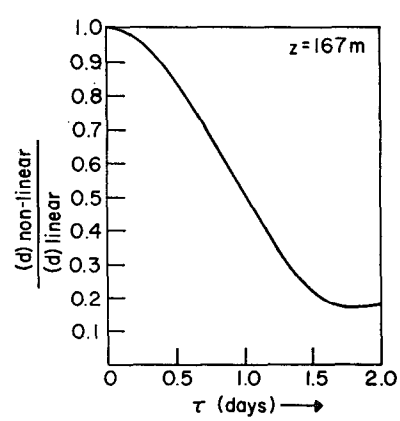

FIG. 3. Time variation of the ratio of the frontal scales at $z=167$ m.

scale to zero at a finite time. A similar analysis can be carried out for the present case. The curve in Fig. 3 suggests that if Δy, Δz could be made arbitrarily small, then a discontinuity would form at about $t=42$ hr. The quasi-geostrophic solution becomes discontinuous only at the surface and only as t approaches infinity.

Let us now examine the vertical structure of the frontal zone. All of the solutions satisfy the odd symmetry relation

$$s(y,z)=-s(-y,H-z), \tag{5.4}$$

where $s=u$, v, w or θ. Therefore, only the lower half plane will be shown for each field. Fig. 4 contains cross sections of θ', where θ' is the departure from the horizontally averaged initial potential temperature $\bar{\theta}_I$. The initial θ' which is independent of z is shown in Fig. 4a. The linear prediction at $t=30$ hr is depicted in Fig. 4b. The symmetry about $y=0$ is evident and the solution is clearly approaching the analytic quasi-geostrophic solution which is shown in Fig. 3 of the paper by Williams and Plotkin (1968). Fig. 4c contains the nonlinear prediction at $t=30$ hr and the tilt in the frontal zone is in the proper sense. At the surface the frontal zone is located at approximately the point where

$$v+V=0. \tag{5.5}$$

The temperature gradients near the surface are much larger in the nonlinear than in the linear prediction. However, in the middle of the region at $z=4.5$ km the temperature gradients in both predicted fields are nearly equal to the initial gradients.

Fig. 5 contains cross sections of the $-u$ component of the wind. The initial field [Eq. (4.3)], given in Fig. 5a, represents a broad jet with the maximum speed at $y=0$, $z=0$. The linear solution which is shown in Fig. 5b at $t=30$ hr retains symmetry about $y=0$. The maximum wind speed has increased and the width of the jet has decreased. The nonlinear solution which is depicted in Fig. 5c is asymmetric about $y=0$. The maximum speed is about the same as for the linear solution, but the shear is much larger on the warm side of the jet. This zone of large cyclonic vorticity is closely associated with the zone of maximum temperature gradient.

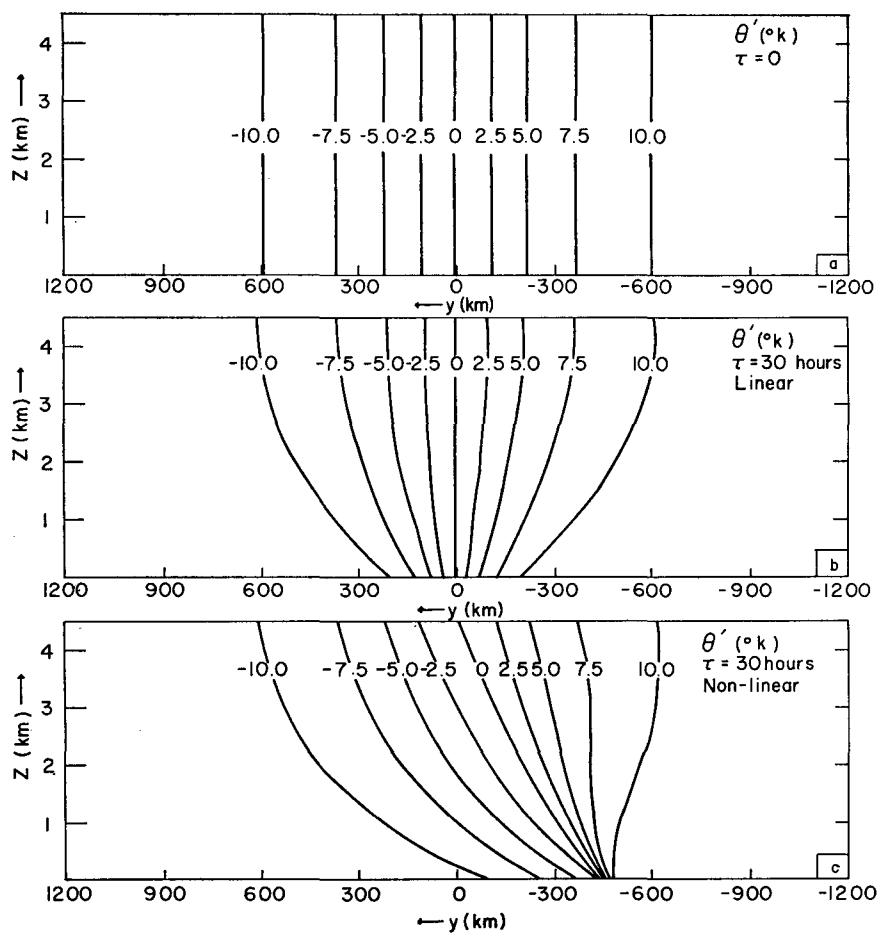

FIG. 4. The θ' field as a function of y and z. Fig. 4a contains the initial field, 4b the linear prediction at $t=30$ hr and 4c the nonlinear prediction at $t=30$ hr.

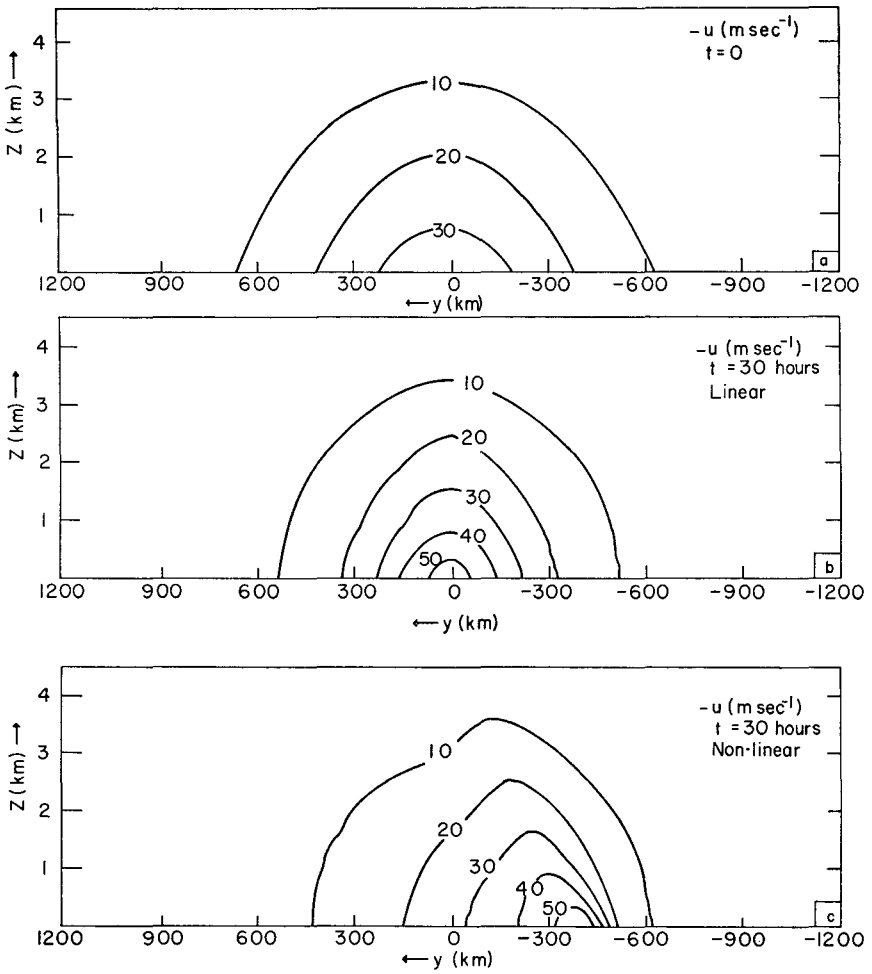

FIG. 5. Same as Fig. 4 except for the u field.

The streamfunction for the circulation in the y-z plane as defined by (4.9) satisfies the even symmetry condition

$$\Psi(y,z)=\Psi(-y,H-z). \tag{5.6}$$

The computed Ψ field at $t=30$ hr is shown for the non-linear case in Fig. 6. The circulation is thermally direct with rising motion in the warm air and sinking motion in the cold air. It can be seen that the frontal zone is immersed in a region of horizontal convergence, and this contributes to the frontogenesis process.

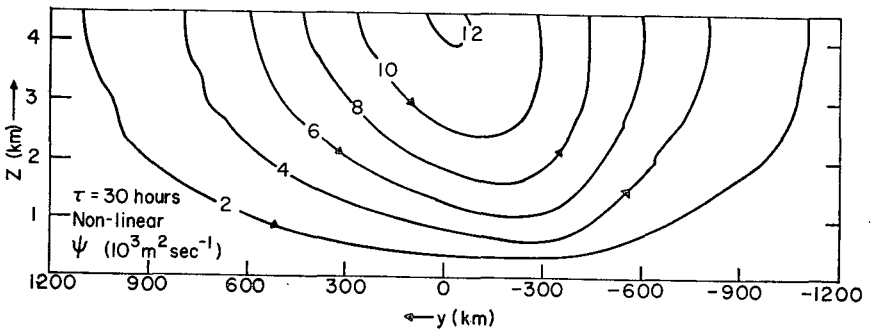

FIG. 6. The streamfunction as a function of y and z at $t=30$ hr from the nonlinear solution. The velocity components are given by $v=-\partial\Psi/\partial y$ and $w=\partial\Psi/\partial y$.

6. Conclusions

We have examined frontogenesis which is forced by a nondivergent horizontal wind field which contains stretching deformation. Quasi-geostrophic solutions for this wind field have been obtained by Stone (1966) and Williams and Plotkin (1968), and these solutions are physically unrealistic in certain respects. The quasi-geostrophic equations neglect advections of momentum and temperature departure (θ') by the divergent circulation. Thus, vertical deformation effects are not properly represented in the quasi-geostrophic equations. The vertical deformation is completely represented when the hydrostatic primitive equations are used. Solutions obtained from the linearized primitive equations are equivalent to the quasi-geostrophic solutions except near the boundaries. The linear and nonlinear primitive equations were solved using the same finite-difference approximations and the solutions were compared. The nonlinear equations predict the rapid development of a sloping frontal zone, while the linear equations give a zone with no tilt. The tilt in the nonlinear solutions gives rise to cyclonic vorticity in the frontal zone which cannot occur in the linear solutions. This tilt gives a temperature field which does not contain the superadiabatic region which occurs in the quasi-geostrophic solutions. The frontogenesis rate is greater in the nonlinear solutions and the results strongly suggest the formation of a discontinuity within a finite period of time. The linear equations produce discontinuities only at $z=0$ and only as $t \rightarrow \infty$. Hoskins (1971) has recently obtained analytic solutions to the balance equations for the deformation wind field used in this paper. Although he used different initial conditions his results are very similar to our nonlinear predictions, and he demonstrates the formation of a discontinuity within a finite period of time. These studies show that the nonlinear equations remove the unrealistic features in quasi-geostrophic frontogenesis.

We now discuss the process by which the tilt develops and by which the frontogenesis rate is increased in the nonlinear solutions. The initial v field advects the frontal zone toward warm air at low levels and cold air at high levels. A limiting position is reached when the v field balances the deformation velocity. This tilt places the frontal zone in a region of cyclonic shear as is seen in Fig. 1. The divergent circulation also shifts, but the line of maximum divergent speed always has a greater slope than the line of maximum temperature gradient. This gives horizontal convergence at the point of maximum temperature gradient, and this increases the frontogenesis rate. This is a nonlinear effect which is not present in the quasi-geostrophic equations. This same process was observed by Williams (1967) in his nonlinear study of frontogenesis arising from a shearing deformation field. These results and the results obtained by Hoskins (1971) suggest that most fronts are formed through this process although other effects may be important in some cases.

Further studies of frontogenesis should include eddy diffusions of heat and momentum. This would permit the formation of quasi-steady frontal zones (see Welander, 1963).

Acknowledgments. The author wishes to thank Prof. G. J. Haltiner for reading the manuscript and for making several useful comments on it. The manuscript was carefully typed by Mrs. Nancy Dean. This research was recently supported by the Navy Weather Research Facility and the Foundation Research Program at the Naval Postgraduate School and in the summer of 1967 by the National Science Foundation under Grant GA-849 at the University of California at Los Angeles. The numerical computations were performed by the Computer Facility at the Naval Postgraduate School and by the University of Utah Computer Center.

REFERENCES

Arakawa, A., 1962: Non-geostrophic effects in the baroclinic prognostic equations. *Proc. Intern. Symp. Numerical Weather Prediction*, Tokyo, 161–175.

——, 1966: Computational design for long-term numerical integration of the equations of fluid motion: Two-dimensional incompressible flow. Part I. *J. Comput. Phys.*, **1**, 119–143.

Charney, J. G., 1962: Integration of the primitive and balance equations. *Proc. Intern. Symp. Numerical Weather Prediction*, Tokyo, 131–152.

Hoskins, B. J., 1971: Atmospheric frontogenesis models: Some solutions. *Quart. J. Roy. Meteor. Soc.*, **97**, 139–153.

Lilly, D. K., 1965: On the computational stability of numerical solutions of time-dependent non-linear geophysical fluid dynamics problems. *Mon. Wea. Rev.*, **93**, 11–26.

Ogura, Y., and J. G. Charney, 1962: A numerical model of thermal convection in the atmosphere. *Proc. Intern. Symp. Numerical Weather Prediction*, Tokyo, 431–452.

Phillips, N. A., 1960: On the problem of initial data for the primitive equations. *Tellus*, **12**, 121–126.

——, 1963: Geostrophic motion. *Rev. Geophys.*, **1**, 123–176.

Platzman, G. W., 1954: The computational stability of boundary conditions in numerical integration of the vorticity equation. *Arch. Meteor. Geophys. Bioklim.*, **7**, 29–40.

Stone, P. H., 1966: Frontogenesis by horizontal wind deformation fields. *J. Atmos. Sci.*, **23**, 455–465.

——, 1969: The meridional structure of baroclinic waves. *J. Atmos. Sci.*, **26**, 376–389.

Welander, P., 1963: Steady plane fronts in a rotating fluid. *Tellus*, **15**, 33–43.

Williams, R. T., 1967: Atmospheric frontogenesis: A numerical experiment. *J. Atmos. Sci.*, **24**, 627–641.

——, 1968: A note on quasi-geostrophic frontogenesis. *J. Atmos. Sci.*, **25**, 1157–1159.

——, and J. Plotkin, 1968: Quasi-geostrophic frontogenesis. *J. Atmos. Sci.*, **25**, 201–206.